Journal of Systems Engineering and Electronics
Vol. 32, No. 3, June 2021, pp.596 – 606

Integrated method for measuring distance and time difference between small satellites

ZHU Yaowei[1], XU Zhaobin[1,*], JIN Xiaojun[2], GUO Xiaoxu[1], and JIN Zhonghe[2]

1. Micro-Satellite Research Center, Zhejiang University, Hangzhou 310027, China;
2. School of Aeronautics and Astronautics, Zhejiang University, Hangzhou 310027, China

Abstract: The advancement of small satellites is promoting the development of distributed satellite systems, and for the latter, it is essential to coordinate the spatial and temporal relations between mutually visible satellites. By now, dual one-way ranging (DOWR) and two-way time transfer (TWTT) are generally integrated in the same software and hardware system to meet the limitations of small satellites in terms of size, weight and power (SWaP) consumption. However, studies show that pseudo-noise regenerative ranging (PNRR) performs better than DOWR if some advanced implementation technologies are employed. Besides, PNRR has no requirement on time synchronization. To apply PNRR to small satellites, and meanwhile, meet the demand for time difference measurement, we propose the round-way time difference measurement, which can be combined with PNRR to form a new integrated system without exceeding the limits of SWaP. The new integrated system can provide distributed small satellite systems with on-orbit high-accuracy and high-precision distance measurement and time difference measurement in real time. Experimental results show that the precision of ranging is about 1.94 cm, and that of time difference measurement is about 78.4 ps, at the signal to noise ratio of 80 dBHz.

Keywords: time difference measurement, time synchronization, inter-satellite ranging, satellite formation autonomous flying.

DOI: 10.23919/JSEE.2021.000051

1. Introduction

In recent years, the use of microelectronics and microsystems technologies, especially the application of compact commercial-off-the-shelf (COTS) components, have dismissed the trade-off between the functionality and the limitations of small satellites in terms of size, weight and power (SWaP) consumption [1–3]. As a result, the manufacturing cost and launch price per small satellite are much cheaper and the development time is much shorter than deploying a traditional monolithic satellite. These characteristics make small satellites very suitable for new scientific and technological research in the satellite field [1,4]. For instance, adopting small satellites in a distributed satellite system (DSS) [5,6] such as satellite formations, swarms, and constellations can dramatically reduce the overall cost and deployment time [2,7].

Compared with a single satellite system, a DSS is more reliable and redundant, with wider surveillance areas, and the mission design can be more flexible, but one of the challenges is high-precision relative navigation [8,9]. It is essential to coordinate the spatial and temporal relations between each two mutually visible satellites in a DSS. On the one hand, an accurate inter-satellite ranging system is required for avoiding satellite collisions [10], maintaining a distributed configuration or fulfilling specific tasks [11]. On the other hand, an accurate inter-satellite time difference measurement system is required because the states of the satellites should be coordinated to obey the event schedule correctly, and the measurement data of different satellites should be marked with a unified timestamp, otherwise, the measurement result cannot be accurate enough [5]. Satellites TerraSAR-X and TanDEM-X formed the first configurable synthetic aperture radar (SAR) interferometer employing autonomous formation flying in 2010 [12]. The satellite formation is equipped with a TanDEM-X autonomous formation flying (TAFF) system, which can take over the in-plane formation maintenance activities from the ground segment [13]. TAFF utilizes the data from on-board global positioning system (GPS) receivers to control the inter-satellite distance, and the typical formation control accuracy is 30 m. In the gravity recovery and climate experiment (GRACE [14]) mission, the inter-satellite distance is measured by dual one-way ranging [15] (DOWR) method, and two GPS receivers are used to provide unified timestamps for each of those one-way measurements. To ensure high ranging ac-

Manuscript received March 22, 2020.
*Corresponding author.
This work was supported by the National Natural Science Foundation of China (61401389).

curacy, the timestamp synchronization accuracy is further improved by post-interpolation processing. If the time-tag error is 200 ps, the overall accuracy of the range rate is well below 1 μm/s [15]. In the gravity recovery and interior laboratory (GRAIL) mission [16] which is like GRACE, but where GPS service is not available, a pair of dedicated S-band transponders [17] is used for inter-satellite two-way time transfer (TWTT) [18].

For a DSS composed of small satellites, combining inter-satellite ranging and time synchronization and implementing on the same device can reduce the payloads. The combination can be achieved by using the modern digital transceiver design based on field programmable gate array (FPGA). In [19], a system that combined TWTT and the dual-frequency carrier ranging method was illustrated, and the ambiguity of carrier ranging was resolved by using pseudo-noise (PN) code ranging. The precision of ranging and time synchronization are irrelevant, which are 1 cm and (8.3/8) ns respectively. In [20], a precise ranging and time synchronization system was implemented based on DOWR. The time difference measurement method is equivalent to TWTT. And the precision of ranging and time synchronization are 1.038 m and 3.46 ns respectively when the two terminals using different frequency references, 2.788 mm/9.3 ps when using a common frequency reference. It seems that the frequency deviation has a great influence on the measurement precision. Inspired by [20] and [21], both DOWR and TWTT can be implemented into an inter-satellite direct-sequence spectrum spread (DSSS) communication system, thereby forming a comprehensive inter-satellite measurement and communication system. However, the measurement precision and accuracy of DOWR rely on the synchronization accuracy of the measurement time of the two one-way measurements [22,23]. It is the same for TWTT unless the two signal transmission paths remain reciprocal and stationary over time [18,24]. It has been analyzed in the GRAIL mission that the time difference measurement error caused by unsynchronized measurement time is bound to several nanoseconds, and the error caused by the non-reciprocal transmission paths is about hundreds of nanoseconds [25].

PN regenerative ranging [26] (PNRR) is a coherent ranging method which is widely used in missions of deep space exploration. The ranging precision and accuracy of PNRR are irrelevant to the accuracy of time synchronization and the clock source deviation. Additionally, the composite PN sequence used by PNRR has a higher sequence transition density than that of the PN sequence used by a DSSS system, such as Gold code. Thus, the measurement system based on composite PN code can achieve a better measuring precision and accuracy than the measurement system based on the DSSS system by adopting the non-commensurate sampling technique and the double-loop tracking structure [27].

In this paper, we propose the round-way time difference measurement (RWTDM) method based on PNRR to form a new integrated inter-satellite distance and time difference measuring system for micro-satellite formations. The new integrated system enables micro-satellites to measure inter-satellite distance and time difference in real time with high-precision and high-accuracy, without breaking the SWaP constraints. Experimental results show that when the signal power-over-noise power spectral density ratio (SNR) is 80 dBHz and the chip rate is 1 Mbps, the ranging precision is 5.76 cm and the frequency offset measurement precision of 1 s interval is about 1 Hz under the condition that the two test boards use separate clocks, while the ranging precision is 1.94 cm and the time difference measuring precision is 78.4 ps under the condition of using a common clock. The common clock experiment is an equivalent to the situation that the time difference compensation system (TDCS) [21] is applied. And the measurement precision can be further improved if the pseudo-range is smoothed with carrier phase [28].

The rest of this paper is organized as follows. Section 2 is the introduction of PNRR and RWTDM integrated system, as well as the explanation of working principles. Section 3 is the implementation and performance analysis of the measurements. Section 4 presents the experimental results, and Section 5 presents the conclusions.

2. System introduction

2.1 System overview

We have successfully implemented the PNRR and RWTDM integrated system in the inter-satellites communication transceivers (shown in Fig. 1) of two micro-satellites. Fig. 2 shows the software framework, where transceiver M-sat serves as the position and time reference of transceiver S-sat, and the latter is responsible for initiating the measurements. The baseband processing (BBP) module is for digital modulation and demodulation, besides, both M-sat and S-sat maintain a local composite PN sequence generator driven by local oscillator (OSC), track the incoming PN sequence through the code tracking loop (CTL) [26], and measure the phase difference between the local PN sequence and the incoming PN sequence. When ready to start measurement, S-sat transmits its local PN sequence to M-sat. However, M-sat does not do so, instead, it echoes the S-sat PN sequence back

to S-sat as soon as the sequence is regenerated. The measurement of S-sat is ρ_s, which indicates the round-way delay of the S-sat PN sequence. And the measurement of M-sat is ρ_m, indicating the one-way phase difference (in seconds) between PN sequences of M-sat and S-sat. Then, one-way measurement ρ_m is transmitted to S-sat through the inter-satellite communication channel for calculating the inter-satellite time difference in real time, while the inter-satellite distance is calculated by using ρ_s.

Fig. 1 Micro-satellite communication transceiver

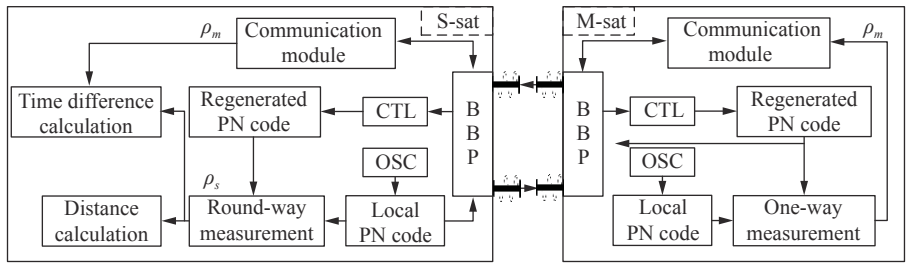

Fig. 2 System software framework

2.2 Principles of PNRR and RWTDM

Generally, a one-way phase difference measurement contains information about the inter-satellite distance and time difference, but only the distance information is included in the round-way phase difference measurement of PNRR. Thus, the time difference can be decoupled from the one-way measurement by using the round-way measurement.

To illustrate the principles of PNRR and RWTDM in detail, assume that M-sat and S-sat generate the local PN sequences at equal chip rate f_{PN}, and the time of M-sat is ahead that of S-sat by ΔT. Then, the PN signal phase of M-sat and S-sat at time t can be expressed as

$$\varphi_m(t) = 2\pi f_{\mathrm{PN}} t, \tag{1}$$

$$\varphi_s(t) = 2\pi f_{\mathrm{PN}}(t - \Delta T). \tag{2}$$

In Fig. 3, the signal phases of M-sat and S-sat are equal to ϕ at time t_1 and t_2, respectively, which are

$$\varphi_m(t_1) = \varphi_s(t_2) = \phi, \tag{3}$$

$$\Delta T = t_2 - t_1. \tag{4}$$

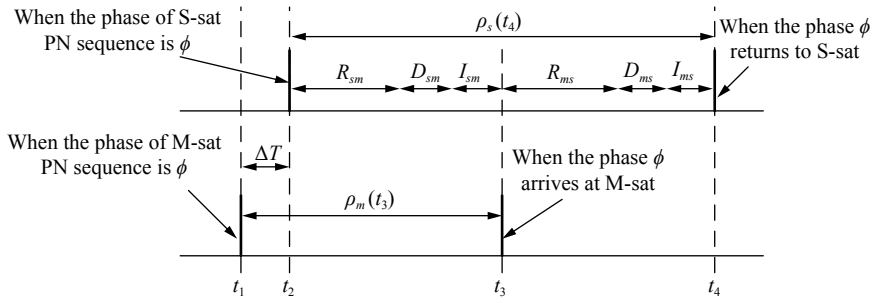

Fig. 3 Measurement process of PNRR and RWTDM

Fig. 3 shows the measurement process of PNRR and RWTDM by tracking the transfer process of phase ϕ that is sent from S-sat. Simply put, phase ϕ leaves S-sat for M-sat at time t_2, arrives at M-sat at time t_3, and also leaves M-sat for S-sat at time t_3. Finally, phase ϕ returns to S-sat at time t_4.

Suppose the measurement of phase difference can be done instantly no matter at M-sat or S-sat and ignore the thermal noise. Then the one-way measurement of M-sat at time t_3 as well as the round-way measurement of S-sat at time t_4 are

$$\rho_m(t_3) = \frac{1}{2\pi f_{\mathrm{PN}}}(\varphi_m(t_3) - \varphi_s(t_2)) = \Delta T + R_{sm} + D_{sm} + I_{sm}, \tag{5}$$

$$\rho_s(t_4) = \frac{1}{2\pi f_{\mathrm{PN}}}(\varphi_s(t_4) - \varphi_s(t_2)) = R_{sm} + R_{ms} + D_{sm} + D_{ms} + I_{sm} + I_{ms}, \tag{6}$$

where R, D and I represent the signal transmission path delay, device delay, and ionospheric delay respectively, with the subscript indicating the path direction.

Observed at S-sat, the forward and backward transmission paths of phase ϕ are reciprocal, since phase ϕ leaves as soon as it reaches M-sat. It is like throwing a weightless ping-pong ball at the speed of light against a wall from S-sat, then it bounces back as soon as it hits the wall and returns to S-sat in the velocity of light, too. In the view of S-sat, the forward path and the backward path of the ping-pong ball are reciprocal with their length equal to the distance between S-sat and the wall at the moment the ping-pong ball hits the wall, no matter the wall is moving or not. Thus, for phase ϕ,

$$R_{sm} = R_{ms}. \tag{7}$$

The delay of phase ϕ at M-sat due to hardware and software processing is considered in the device delay. Thus, according to (6), the measurement equation of inter-satellite distance r is

$$r = \frac{\mathrm{c}}{2}(\rho_s(t_4) - (D_{sm} + D_{ms}) - (I_{sm} + I_{ms})) \tag{8}$$

where c is the velocity of light.

Substitute (8) into (5) to decouple the inter-satellite time difference from the one-way measurements:

$$\Delta T = \rho_m(t_3) - \frac{1}{2}\rho_s(t_4) + \frac{1}{2}(D_{ms} - D_{sm}) + \frac{1}{2}(I_{ms} - I_{sm}). \tag{9}$$

Equation (9) verifies the feasibility of RWTDM in measuring the inter-satellite time difference. It also shows that RWTDM does not require ρ_m and ρ_s to be measured at the same time, which means there is no need to synchronize the measurement time of the two measurements, making RWTDM suitable for working onboard in real time.

3. Implementation and performance analysis

3.1 Implementation of RWTDM

Though RWTDM does not require ρ_m and ρ_s to be measured simultaneously, it is necessary to find the right pair of ρ_m and ρ_s to calculate time difference. We propose a simple and effective way to match ρ_m and ρ_s without recording the measurement time of ρ_m and ρ_s which is useless if the time of S-sat and M-sat has not been synchronized yet. The solution is to control the measurement of ρ_m and ρ_s with a trigger signal delivered by S-sat through the inter-satellite communication channel when the measurement is about to start. The trigger signal is always transferred along with the measuring signal, serving as a label attached to phase ϕ which could be arbitrary. Then M-sat measures ρ_m and echoes the trigger signal back to S-sat as soon as it is received and S-sat measures ρ_s when the trigger signal returns. Eventually, one-way measurement ρ_m and round-way measurement ρ_s that are triggered by the same trigger signal can be used for calculating ΔT.

3.2 Implementation and performance of phase difference measurement

The actual implementation of measuring ρ_s and ρ_m determines how precisely the inter-satellite distance and time difference can be obtained, which involves the selection of measuring signals and the measurement method. In this paper, the Tausworthe, $v = 4$ (T4B) ranging code is used as the measuring signal of the integrated system. The T4B code is composed of a strong clock-code component and five sub-code components, so it is preferable for high measurement accuracy applications [26].

Taking ρ_s as an example, it can be expressed as follows in general:

$$\rho_s(t) = N_s \cdot T_c + n_s \tag{10}$$

where T_c is the chip interval; N and n are the integer ambiguity and the decimal part of phase difference measurement respectively.

The integer ambiguity N can be determined by using Chinese remainder theorem [29,30]. During one measurement process, it is unlikely that N is affected by random noise. On the contrary, the decimal part n is more susceptible to random noise. There are two architectures in [26] for determining n, which are closed loop architecture and open loop architecture.

Fig. 4 shows the open loop architecture, where $x[i]$ is the digital sample of the received measuring signal that is output from the Q branch of the carrier recovery loop. Then $x[i]$ correlates with the local in-phase and mid-phase clock codes respectively. As shown in (11), when in the sine-square mismatched case [26], the open loop architecture has no dependence on CTL, which means the measurement jitter mainly depends on the integration interval T_i and the SNR of the clock code. If a smaller measurement jitter is wanted, T_i can be increased, without modifying the loop bandwidth of CTL and affecting its tracking performance. Consequently, the open loop architecture is preferable.

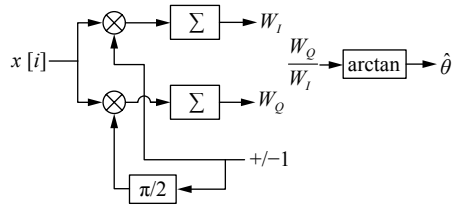

Fig. 4 Open loop architecture

$$\sigma_o = \frac{1}{8f_{clk}}\sqrt{\frac{1}{T_i}\frac{N_0}{P_{clk}}} \tag{11}$$

where f_{clk} is the frequency of the clock-component code, $f_{clk} = 1/2T_c$, and P_{clk}/N_0 is the SNR of the incoming signal.

Thus, the jitters of one-way measurement ρ_m and round-way measurement ρ_s are

$$\sigma_{\rho_m} = \frac{T_c}{4}\sqrt{\frac{1}{T_i}\left(\frac{N_0}{P_{clk}}\right)_m}, \tag{12}$$

$$\sigma_{\rho_s} = \frac{T_c}{4}\sqrt{\frac{1}{T_i}\left[\left(\frac{N_0}{P_{clk}}\right)_m + \left(\frac{N_0}{P_{clk}}\right)_s\right]}. \tag{13}$$

Then, according to (8) and (9), the measurement jitters of inter-satellite distance and inter-satellite time difference are

$$\sigma_r = \frac{cT_c}{8}\sqrt{\frac{1}{T_i}\left[\left(\frac{N_0}{P_{clk}}\right)_m + \left(\frac{N_0}{P_{clk}}\right)_s\right]}, \tag{14}$$

$$\sigma_{\Delta T} = \frac{T_c}{8}\sqrt{\frac{1}{T_i}\left[5\left(\frac{N_0}{P_{clk}}\right)_m + \left(\frac{N_0}{P_{clk}}\right)_s\right]}. \tag{15}$$

3.3 Error analysis and calibration

As shown in (8) and (9), to accurately measure the distance and time difference, the device delay and ionospheric delay have to be calibrated. Besides, the derivation of (8) and (9) is based on the assumptions that M-sat and S-sat generate their own PN sequences at the same chip rate f_{PN}, and the phase difference is measured instantly. These assumptions do not accord with the actual situation. In fact, the frequency drift of oscillators and the frequency offset between them, as well as the time taken by the phase difference measurement, will cause deviations between the measured values and their true values.

3.3.1 Device delay and ionospheric delay calibration

Comparing (8) and (9) with the distance measurement equation in [15] and the time difference measurement equation in [18], respectively, it can be found that the effects of device delay and ionospheric delay on PNRR and RWTDM are the same as on DOWR and TWTT. The device delays and ionospheric delays of the two signal transfer paths are added together for ranging but differentiated for time difference measuring.

D_{sm} in (8) and (9) is composed of the transmission delay of S-sat $D_{tx,s}$ and reception delay of M-sat $D_{rx,m}$, and D_{ms} is composed of the transfer delay of M-sat $D_{tx,m}$ and the receive delay of S-sat $D_{rx,s}$. In [31], a delay calibration device that contained a frequency mixer was used to transform the signal from the transmitting port of S-sat to its receiving port, then the self-ranging result was equal to the delay of calibration board plus the transmission delay and reception delay of the ranging board. Therefore, this method is useful for determining the sum of D_{sm} and D_{ms}, but useless for determining the difference. In [32], a calibration device called satellite simulator was used for measuring the transmission delay and the reception delay of the earth station separately. Using this method, $D_{tx,s}$, $D_{rx,s}$, $D_{tx,m}$ and $D_{rx,m}$ can be measured one by one, thus the sum of D_{sm} and D_{ms} or difference between D_{sm} and D_{ms} can be easily got, too.

The ionospheric effects cannot be avoided in the near-earth space. For ranging, the ionospheric delays on the two paths always add up. However, for time difference measuring, the ionospheric delays can be offset if the paths are symmetric. In [15] and [33], the dual-frequency method was used for eliminating the ionosphere effect. In GPS, the L1 and L2 signals can be combined to model the ionospheric delay [34]. In [35], the Klobuchar model was used for ionospheric delay calibration in a single frequency global navigation satellite system (GNSS). According to [36], the correction accuracy of the dual-frequency method is the highest, followed by the grid method and the Klobuchar model. Thus, the dual-frequency method should be utilized for high-accuracy ranging and time synchronization.

Let f_1 and f_2 denote the dual frequencies that are used, ρ_1 and ρ_2 denote the corresponding measurements, and ρ denote the ionosphere-free measurement. Then the ionosphere effect can be eliminated by using the combination [15] as follows:

$$\rho = \frac{f_1^2\rho_1 - f_2^2\rho_2}{f_1^2 - f_2^2}. \tag{16}$$

3.3.2 Oscillator frequency offset and drift error

Driven by non-ideal oscillators, the instantaneous chip rate of the PN sequence generated by M-sat and S-sat can be modeled as follows:

$$f_m(t) = f_{\mathrm{PN}} + F_m + \int \alpha_m(t)\mathrm{d}t, \tag{17}$$

$$f_s(t) = f_{\mathrm{PN}} + F_s + \int \alpha_s(t)\mathrm{d}t, \tag{18}$$

where F is the rate offset of the PN sequence, and $\alpha(t)$ is the rate drift function.

To analyze the influence of oscillator frequency offset and drift on the measurement error, assume that M-sat and S-sat are relatively static, and ignore the phase difference measurement error, device delay, and ionospheric delay. Then, according to (8) and (9),

$$\hat{r} = \frac{\mathrm{c}}{2}\hat{\rho}_s(t_4), \tag{19}$$

$$\Delta\hat{T} = \hat{\rho}_m(t_3) - \frac{1}{2}\hat{\rho}_s(t_4), \tag{20}$$

where

$$\hat{\rho}_m(t_3) = \frac{1}{f_{\mathrm{PN}}}\int_{t_1}^{t_3} f_m(t)\mathrm{d}t, \tag{21}$$

$$\hat{\rho}_s(t_4) = \frac{1}{f_{\mathrm{PN}}}\int_{t_2}^{t_4} f_s(t)\mathrm{d}t. \tag{22}$$

The ranging error is mainly caused by the deviation between the actual frequency of the S-sat oscillator and the nominal frequency, which is

$$r_{osc,e} = \hat{r} - \frac{\mathrm{c}(t_4 - t_2)}{2} = \frac{\mathrm{c}}{2f_{\mathrm{PN}}}\int_{t_2}^{t_4}\left(F_s + \int_{t_2}^{t}\alpha_s(\tau)\mathrm{d}\tau\right)\mathrm{d}t. \tag{23}$$

For time difference measurement, the error is determined by comparing $\Delta\hat{T}$ with the time difference when the measurement process ends:

$$\Delta T_{osc,e} = \Delta\hat{T} - \Delta T(t_4) = \frac{1}{2f_{\mathrm{PN}}}\int_{t_2}^{t_4}\left(F_s + \int_{t_2}^{t}\alpha_s(\tau)\mathrm{d}\tau\right)\mathrm{d}t - \frac{1}{f_{\mathrm{PN}}}\int_{t_3}^{t_4}\left(F_m + \int_{t_3}^{t}\alpha_m(\tau)\mathrm{d}\tau\right)\mathrm{d}t \tag{24}$$

where

$$\Delta T(t_4) = \frac{1}{2\pi f_{\mathrm{PN}}}(\varphi_m(t_4) - \varphi_s(t_4)). \tag{25}$$

Suppose M-sat and S-sat both use the oscillator with a nominal frequency of 40 MHz, stability of 0.5 ppm, and a drift rate of no more than 1 Hz/s. And the chip rate is 1 Mbps. Thus,

$$F_m, F_s \in (-0.5\ \mathrm{bps}, 0.5\ \mathrm{bps}) \tag{26}$$

$$\alpha_m, \alpha_s \in \left(-\frac{1}{40}\ \mathrm{bps/s}, \frac{1}{40}\ \mathrm{bps/s}\right). \tag{27}$$

On the other hand, the time of a complete measurement process is related to the inter-satellite distance, usually no more than hundreds of milliseconds in the near-earth space. Take the inter-satellite distance of 900 km as an example. Besides, the oscillator frequency drift is a slow process, therefore, it can be regarded as a constant during the short measurement interval. In this case, according to (23) and (24), the maximum ranging error due to the frequency offset of the S-sat oscillator is about 45 cm, and for time difference measurement, the maximum error is about 3 ns.

An effective method for reducing the measurement error of PNRR and RWTDM is to calibrate the measurement results with the exact value of frequency offset and drift. However, it is impossible to measure frequency offset and drift of the oscillators onboard. A lookup table about frequency offset and drift of each oscillator under vacuum circumstances and different temperatures must be established when the measurement system is tested on the ground.

If RWTDM is successfully applied to the time sync system [21] as a time difference measurement module, it is possible to keep

$$F_m = F_s, \tag{28}$$

$$\alpha_m = \alpha_s. \tag{29}$$

Then, the maximum error of measuring time difference is about 0.1 ps, which is negligible. It seems that if the clock frequencies of the two satellites are synchronized, then most of the time difference measurement error can be canceled out. However, the ranging error is not reduced.

3.3.3 Phase difference measurement error

As shown in Fig. 4, the phase difference measurement involves integrating the correlation results of the incoming signal and the local signal in an interval T_i. This design has some advantages, such as reducing the impact of random jitters on the measurement results and improving the measurement precision. However, there are some disadvantages, such as introducing a deviation between the measurement result and the instantaneous value in dynamic scenes.

To assess the phase difference measurement error in dynamic scenes, the impacts due to quantization, oscillator frequency offset and drift are ignored, and the digital measurement system is regarded as an analog system. The clock-code component of T4B is equivalent to a sine or cosine wave after being sinewave shaped. Thus, the incoming signal $x(t)$ can be expressed as

$$x(t) = \cos(2\pi(f_{clk} - f_d)t - \theta_0) \tag{30}$$

where f_d is the Doppler frequency offset, and θ_0 is the phase difference when the measurement starts.

In the sine-square mismatched case [26],

$$W_Q = \int_0^{T_i} x(t)\mathrm{sign}(\sin(2\pi f_{clk}t))\,\mathrm{d}t, \tag{31}$$

$$W_I = \int_0^{T_i} x(t)\mathrm{sign}(\cos(2\pi f_{clk}t))\,\mathrm{d}t. \tag{32}$$

Approximate the square wave with its first harmonic, then,

$$W_Q \approx \int_0^{T_i}\frac{2}{\pi}\sin(2\pi f_d t + \theta_0)\,\mathrm{d}t, \tag{33}$$

$$W_I \approx \int_0^{T_i} \frac{2}{\pi} \cos(2\pi f_d t + \theta_0)\,\mathrm{d}t. \tag{34}$$

Thus, the measured phase difference $\hat{\theta}$ is

$$\hat{\theta} = \arctan\left(\frac{W_Q}{W_I}\right) = \underbrace{(\theta_0 + 2\pi f_d T_i)}_{\theta_{\text{end}}} + \underbrace{(-\pi f_d T_i)}_{\theta_{\text{meas},e}} \tag{35}$$

where θ_{end} represents the phase difference when the measurement ends, and $\theta_{\text{meas},e}$ is the measurement error. It turns out that the measurement of the phase difference will always deviate from the instantaneous value in dynamic scenes, and the amount is relevant to the relative velocity between the two satellites and the integration interval T_i.

Suppose there is a dynamic scene with linear uniform motion as shown in Fig. 5. This supposition is reasonable because the relative motion between satellites in a DSS will not change drastically during a short integration interval which is usually hundreds of milliseconds.

Fig. 5 Dynamic scene

According to (35), the one-way phase difference measurement error and round-way phase difference measurement error in seconds are

$$\rho_{e,m} = -\frac{\pi f_{d,sm} T_i}{2\pi f_{clk}} = -\frac{uT_i}{2\mathrm{c}}, \tag{36}$$

$$\rho_{e,s} = -\frac{\pi f_{d,ms} T_i}{2\pi f_{clk}} = -\frac{uT_i}{\mathrm{c}} \tag{37}$$

where

$$f_{d,sm} = \frac{u}{\mathrm{c}} f_{clk}, \tag{38}$$

$$f_{d,ms} = \frac{u}{\mathrm{c}} f_{clk} + \frac{u}{\mathrm{c}}\left(1 - \frac{u}{\mathrm{c}}\right) f_{clk} \approx \frac{2u}{\mathrm{c}} f_{clk}. \tag{39}$$

Then, the measurement error of inter-satellite distance and time difference are

$$r_{\text{meas},e} = \frac{\mathrm{c}}{2}\rho_{e,s} = -\frac{uT_i}{2} \tag{40}$$

$$\Delta T_{\text{meas},e} = \rho_{e,m} - \frac{1}{2}\rho_{e,s} = 0. \tag{41}$$

Equation (40) shows that the error of inter-satellite distance measurement can be calibrated if the relative speed is known, and (41) shows that the measurement error of inter-satellite time difference is nearly zero because any error that appear in one-way measurement will double in round-way measurement and could be canceled out by then.

4. System demonstration

To verify the feasibility of PNRR and RWTDM integrated system, we carry out some experiments in the testbench as shown in Fig. 6. In these experiments, two micro-satellite transceivers used for inter-satellite communication and measurement are adopted, one is labeled as S-sat and the other as M-sat. It should be noted that the examination of the measurement accuracy is absent in this paper. We mainly focus on the measurement precision of the integrated system.

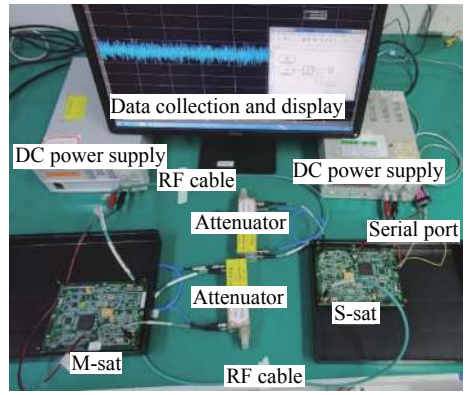

Fig. 6 Testbench

Fig. 7 shows the schematic diagram for separate clock experiments, where S-sat and M-sat are driven by independent clock sources. This testbench simulates the actual application scenario. The nominal frequency of the two OSCs is 40 MHz. Generally, offset exists between the frequencies of the two OSCs. And the offset makes the time difference measurement a linear function of time, while the distance measurement is a constant with additive noise.

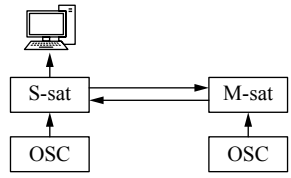

Fig. 7 Testbench of separate clock experiments

Fig. 8 is an example of the measurement results when SNR is 70 dBHz, and the mean values are removed for better display. The measurement results of PNRR are the evidence to its immunization to the frequency and time asynchronization between two transceivers.

For PNRR, the standard deviation of measured values is used to indicate the measurement precision. Fig. 9 shows the measurement precision of PNRR at different SNRs, and the theoretical values are calculated according to (14). The relative deviations between the experimental

values and theoretical values are small in the case of a low SNR and large in the case of a high SNR, and the measurement precision is not significantly improved when the SNR changes from 70 dBHz to 80 dBHz. This is because in these experiments SNR refers only to the ratio between signal power and thermal noise power spectral density (PSD) and does not involve noise of the frequency source. When the SNR is high, the PSD of the frequency source noise overwhelms that of the thermal noise. Thus, the actual SNR within the system bandwidth is lower than its preset value. As a result, the measurement precision in a high SNR is worse than expected. The results of the experiments show that the measurement precision of PNRR is better than 10 cm if the SNR exceeds 65 dBHz.

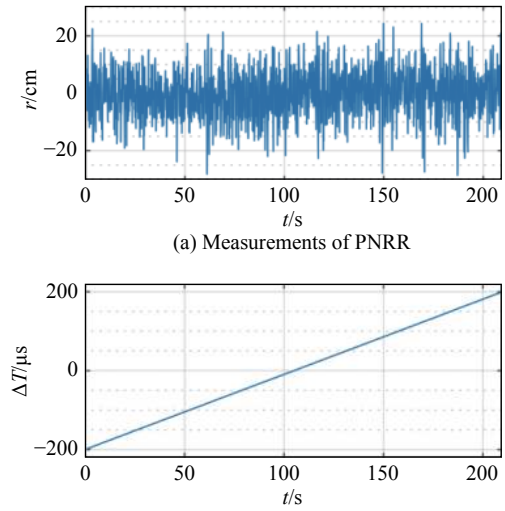

(a) Measurements of PNRR

(b) Measurements of RWTDM

Fig. 8 Measurements of separate clock experiments when SNR is 70 dBHz

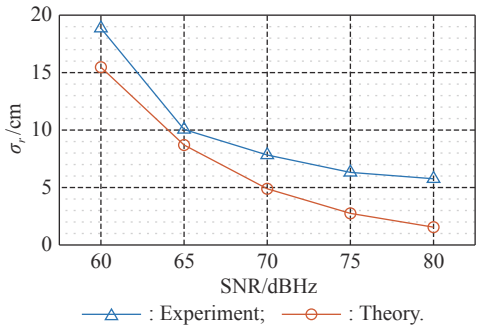

Fig. 9 Measurement precision of PNRR of separate clock experiments

For RWTDM, the standard deviation of the measured data is meaningless, but the slope of the measured curve equals the normalized frequency offset between the two independent OSCs, so Allan standard deviation can be used for estimating how well the RWTDM measurements reflect the frequency offset. Fig. 10 shows the Allan standard deviation curve of RWTDM measurements at different SNRs. Allan standard deviation reflects the normalized frequency offset measurement precision, but it seems that there is no clear relationship between the measurement precision and the SNR. Sometimes the measurement precision increases as the SNR increases, sometimes the opposite is true, depending on the value of τ. The value of τ is an integer multiple of T_i. In the experiments, T_i equals 0.1049 s. Table 1 lists the measurement precision of frequency offset at different SNRs when τ is about 1 s.

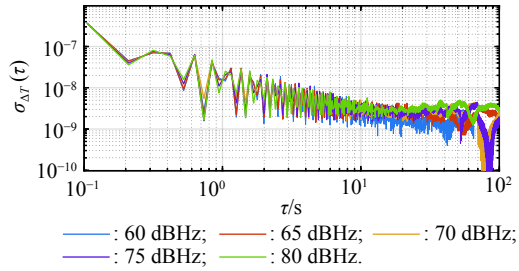

Fig. 10 Allan standard deviation of RWTDM measurements

Table 1 Frequency offset measurement precision

SNR/dBHz	STD of frequency offset/Hz	
	$\tau = 9T_i$	$\tau = 10T_i$
60	0.690	0.578
65	0.620	0.645
70	0.451	0.820
75	0.438	0.834
80	0.302	1.008

To evaluate the measurement precision of RWTDM, the clock frequencies of S-sat and M-sat must be synchronized. We have not finished replacing the time difference measurement module of the time sync system [21] yet, instead, we try to use a common clock source to drive S-sat and M-sat as shown in Fig. 11. Of course, this approximation is a little over ideal, but it is appropriate to examine the upper bound of measurement precision that RWTDM can achieve.

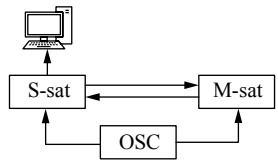

Fig. 11 Testbench of common clock experiments

Fig. 12 is an example of the measurement results when the SNR is preset to 70 dBHz, and the mean values are removed for better display. Fig. 13 and Fig. 14 show the measurement precision of PNRR and RWTDM at different SNRs, respectively. The best case is at the SNR of

80 dBHz, in which the measurement precision of PNRR is 1.94 cm, and that of RWTDM is 78.4 ps.

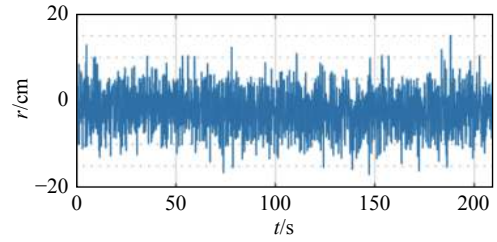

(a) Measurements of PNRR

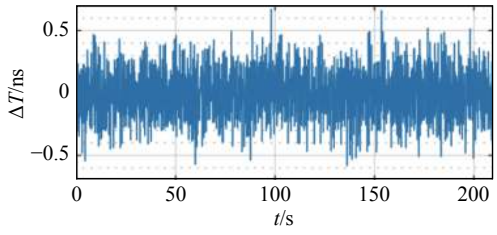

(b) Measurements of RWTDM

Fig. 12 Measurements of common clock experiments when SNR is 70 dBHz

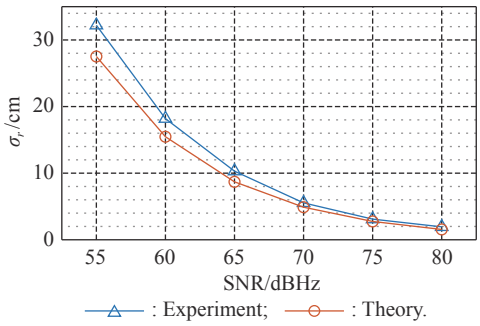

Fig. 13 Measurement precision of PNRR of common clock experiments

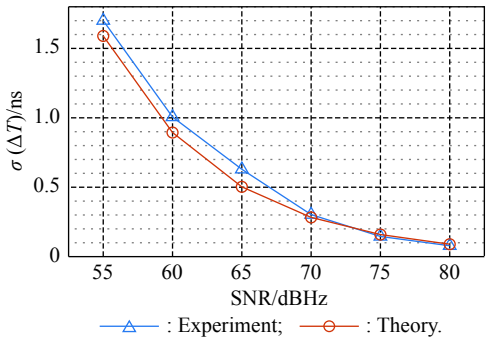

Fig. 14 Measurement precision of RWTDM

Comparing Fig. 13 and Fig. 9, it can be found that the measurement precision of PNRR is improved in the case of a high SNR because the frequency synchronization between S-sat and M-sat allows most of the frequency source noise to be eliminated. For example, the ranging precision improves to 5.54 cm at an SNR of 70 dBHz. As shown in Fig. 14 and Table 2, the results of the common clock experiments fit well with the theoretical estimates. The experimental measurement precision is a little better than theoretical prediction at SNRs of 75 dBHz and 80 dBHz. It seems that the actual SNR exceeds the preset value by no more than 1 dBHz, which is reasonable because the minimum adjustment resolution of SNR in the experiments is 1 dBHz. The data about TWTT listed in Table 2 is got from [21]. The comparison between RWTDM and TWTT shows that the measurement precision of RWTDM is comparable to the theoretical measurement precision of TWTT at the same SNR. However, as illustrated in Section 1, the integration of PNRR and RWTDM is better than the integration of DOWR and TWTT.

Table 2 Comparison between RWTDM and TWTT

SNR/dBHz	Precision of RWTDM/ps		Precision of TWTT/ps	
	Theory	Experiment	Theory	Experiment
65	502.7	629.4	446.1	770.7
70	282.5	302.9	262.2	487.5
75	159.0	145.4	150.6	305.9
80	89.4	78.4	90.07	186.1

5. Conclusions

In this paper, we propose a new inter-satellite time difference measurement method, RWTDM, based on PNRR. The measurement equation proves the feasibility of RWTDM theoretically. We integrate RWTDM and PNRR together and implement it in the micro-satellite transceivers. The new integrated system can provide micro-satellites onboard distance measurement and time difference measurement simultaneously with a high precision and a high accuracy in real time, without the need of complex post data processing algorithms or assistance from other satellite systems. The system can be applied to missions such as earth observation or planetary science that uses small satellites and meets the needs of on-orbit inter-satellite distance maintenance and scientific data synchronization. Besides, according to the fact that PNRR can be used to measure the long distance between a deep space probe and its supporting ground station, RWTDM can be used to measure the time difference between the deep space probe and the ground station. Some of the significant implementation details of the system have been described, and the performance is also analyzed. It turns out that errors caused by frequency drift and offset of the oscillators, and inter-satellite relative motion on the two signal transmission paths are added together for PNRR but differentiated for RWTDM. Finally, the results of the separate clock experiments show that

PNRR as a coherent ranging method does not require the time between two satellites to be synchronized to achieve high-accuracy ranging, even though there is a deviation between the clock frequencies. The best result of ranging precision is 5.76 cm at the SNR of 80 dBHz. RWTDM reliably shows that the time error of the two satellites increases with time when driven by clock sources of different frequencies. Further, to assess the measurement precision of RWTDM, we carry out the common clock experiments. The experimental results show that if clock frequencies of the two involved satellites are synchronized, the measurement precision of time difference is 78.4 ps, while the ranging precision is 1.94 cm, at the SNR of 80 dBHz.

References

[1] POGHOSYAN A, GOLKAR A. CubeSat evolution: analyzing CubeSat capabilities for conducting science missions. Progress in Aerospace Sciences, 2017, 88: 59–83.

[2] DAVOLI F, KOUROGIORGAS C, MARCHESE M, et al. Small satellites and CubeSats: survey of structures, architectures, and protocols. International Journal of Satellite Communications and Networking, 2019, 37(4): 343–359.

[3] RADHAKRISHNAN R, EDMONSON W W, AFGHAH F, et al. Survey of inter-satellite communication for small satellite systems: physical layer to network layer view. IEEE Communications Surveys and Tutorials, 2016, 18(4): 2442–2473.

[4] BANDYOPADHYAY S, SUBRAMANIAN G P, FOUST R, et al. A review of impending small satellite formation flying missions. Proc. of the 53rd AIAA Aerospace Sciences Meeting, 2015: 1−17.

[5] ZHANG H, GURFIL P. Distributed control for satellite cluster flight under different communication topologies. Journal of Guidance, Control, and Dynamics, 2016, 39(3): 617–627.

[6] RUIZ-DE-AZUA J A, CALVERAS A, GOLKAR A, et al. Proof-of-concept of a federated satellite system between two 6-unit CubeSats for distributed earth observation satellite systems. Proc. of the IEEE International Geoscience and Remote Sensing Symposium, 2019: 8871–8874.

[7] BOUWMEESTER J, GUO J. Survey of worldwide pico- and nanosatellite missions, distributions and subsystem technology. Acta Astronautica, 2010, 67(7): 854–862.

[8] WANG D W, WU B L, POH E K. Satellite formation flying. Singapore: Springer, 2017.

[9] NARYTNIK T, RASSAMAKIN B, PRISYAZHNY V, et al. Coverage area formation for a low-orbit broadband access system with distributed satellites. Proc. of the International Conference on Information and Telecommunication Technologies and Radio Electronics, 2018: 1–4.

[10] WAN B, CHEN H, WANG W Y, et al. Collision avoidance engineering design for satellite formation flying. Proc. of the IEEE CSAA Guidance, Navigation and Control Conference, 2018: 1–6.

[11] XU M, HE Y C, YU K. A software architecture design for autonomous formation flying control. IEEE Trans. on Aerospace and Electronic Systems, 2017, 53(6): 2950–2962.

[12] MOREIRA A, KRIEGER G, FIEDLER H, et al. TanDEM-X: a satellite formation for high resolution radar interferometry. Proc. of the 57th International Astronautical Congress, 2006: 1−8.

[13] ARDAENS J S, KAHLE R, SCHULZE D. In-flight performance validation of the TanDEM-X autonomous formation flying system. International Journal of Space Science and Engineering, 2014, 2(2): 1–11.

[14] TAPLEY B D, BETTADPUR S, WATKINS M, et al. The gravity recovery and climate experiment: mission overview and early results. Geophysical Research Letters, 2004, 31(9): 1–4.

[15] KIM J, TAPLEY B D. Simulation of dual one-way ranging measurements. Journal of Spacecraft and Rockets, 2003, 40(3): 419–425.

[16] HOFFMAN T L. GRAIL: gravity mapping the moon. Proc. of the IEEE Aerospace Conference, 2009: 1–8.

[17] ENZER D G, WANG R T, OUDRHIRI K, et al. In situ measurements of USO performance in space using the twin GRAIL spacecraft. Proc. of the IEEE International Frequency Control Symposium, 2012: 1–5.

[18] KIRCHNER D. Two-way time transfer via communication satellites. Proceedings of the IEEE, 1991, 79(7): 983–990.

[19] PAN L J, JIANG T, ZHOU L Y, et al. A research on high-precision time-synchronization and ranging system between satellites. Proc. of the International Conference on Microwave and Millimeter Wave Technology, 2008: 926–929.

[20] MA H J, WU H B, WU J F, et al. Design and implementation of dual one-way precise ranging and time synchronization system. Proc. of the Joint European Frequency and Time Forum & International Frequency Control Symposium, 2013: 831–834.

[21] XU J L, ZHANG C J, WANG C H, et al. Approach to inter-satellite time synchronization for micro-satellite cluster. Journal of Systems Engineering and Electronics, 2018, 29(4): 805–815.

[22] BERTIGER W, DUNN C, HARRIS I, et al. Relative time and frequency alignment between two low earth orbiters, GRACE. Proc. of the IEEE International Frequency Control Sympposium and PDA Exhibition Jointly with the 17th European Frequency and Time Forum, 2003: 273–279.

[23] KIM J. Measurement time synchronization for a satellite-to-satellite ranging system. Proc. of the International Conference on Control, Automation and Systems, 2007: 190–194.

[24] ZHANG V, PARKER T E, ACHKAR J, et al. Two-way satellite time and frequency transfer using 1 MChips/s codes. Proc. of the 41st Annual Precise Time and Time Interval Meeting, 2009: 371−381.

[25] KRUIZINGA G L H, BERTIGER W I, HARVEY N. Timing of science data for the GRAIL mission, JPL D-75620. Pasadena: Jet Propulsion Laboratory, 2013.

[26] CCSDS 414.0-G-2. Pseudo-noise (PN) ranging systems. Washington, DC: Management Council of Consultative Committee for Space Data Systems, 2014: 1−92.

[27] JIN X J, ZHANG W, MO S M, et al. Optimal regenerative PN code tracking based on non-commensurate sampling and double-loop structure. Electronics Letters, 2019, 55(23): 1254–1255.

[28] MA H J, YAN F F, HOU Z J. Application of algorithm of smoothing pseudo-range with carrier phase to DRTS system. Proc. of the International Conference on Computer Networks and Communication Technology, 2016: 209–213.

[29] WANG B. The application of residues theorem in the com-

plex pseudorandom code range detection system. Radio Eegineering of China, 2004, 34(8): 23–24. (in Chinese)
[30] JIN X J. Study on regenerative pseudo noise ranging and its implementation. Hangzhou, China: Zhejiang University, 2007. (in Chinese)
[31] MENG Z M, XU Z B, JIN X J, et al. On-orbit delay calibration of inter-satellite ranging system and its application for micro-satellite. Journal of Astronautics, 2016, 37(10): 1239–1245. (in Chinese)
[32] MERCK P, ACHKAR J. Design of a Ku band delay difference calibration device for TWSTFT station. IEEE Trans. on Instrumentation and Measurement, 2005, 54(2): 814–818.
[33] HAHN J, BEDRICH S. Ultra-precise clock synchronization of remote atomic clocks with PRARE onboard ERS-2. Proc. of the International Symposium on Spread Spectrum Techniques and Applications, 1996, 2: 867–871.
[34] ALBASHIR A, SAMI K A, AHMEDELTIGANI M. Enhancing the accuracy of GPS point positioning by modeling the ionospheric propagation delay. Proc. of the International Conference on Computer, Control, Electrical, and Electronics Engineering, 2018: 1–7.
[35] MALLIKA I L, RATNAM D V, RAMAN S, et al. A new ionospheric model for single frequency GNSS user applications using Klobuchar model driven by auto regressive moving average (SAKARMA) method over Indian region. IEEE Access, 2020, 8: 54535–54553.
[36] LI D D, XU L X, LI B, et al. Analysis of ionospheric delay correction methods for BeiDou navigation satellite system. Proc. of the 13th IEEE International Conference on Electronic Measurement & Instruments, 2017: 603–608.

Biographies

ZHU Yaowei was born in 1993. He received his B.E. degree from Huazhong University of Science and Technology in 2016. Now, he is a Ph.D. candidate of the Micro-Satellite Research Center, Zhejiang University. His research interests include inter-satellite ranging, time synchronization and communication, as well as constellation networking.

E-mail: zhuyaowei@zju.edu.cn

XU Zhaobin was born in 1984. He received his B.E. and Ph.D. degrees from Zhejiang University in 2008 and 2013, respectively. Now he is an associate researcher of Zhejiang University. He has joined in the Micro-satellite Research Center since he was a graduate student. His research interests include micro-satellite transponder technology, inter-satellite ranging, time synchronization and communication, navigation of micro-satellite formation flying, and constellation networking.

E-mail: zjuxzb@zju.edu.cn

JIN Xiaojun was born in 1977. He received his B.E., M.E. and Ph.D. degrees from Zhejiang University in 2001, 2004 and 2007, respectively. He joined the faculty of Zhejiang University in 2009 and has been an associate professor since 2010. Now he is also a Ph.D. supervisor. His research interests include micro-satellite transponder technology, inter-satellite ranging, time synchronization and communication, and navigation of micro-satellite formation flying.

E-mail: axemaster@zju.edu.cn

GUO Xiaoxu was born in 1997. He received his B.E. degree from Harbin Institute of Technology in 2019. Now he is a Ph.D. candidate of the Mirco-Satellite Research Center, Zhejiang University. His research interests include inter-satellite communication, spread spectrum measurement and control, as well as transponder.

E-mail: guoxx@zju.edu.cn

JIN Zhonghe was born in 1970. He received his Ph.D. degree from Zhejiang University in 1998. Now he is a professor with the School of Aeronautics and Astronautics, Zhejiang University. His research interests include micro-satellite and formation technology, MEMS, inter-satellite communication and measurement technology.

E-mail: jinzh@zju.edu.cn